



CHORUS

This is the accepted manuscript made available via CHORUS. The article has been published as:

Detecting electron-phonon coupling during photoinduced phase transition

Takeshi Suzuki, Yasushi Shinohara, Yangfan Lu, Mari Watanabe, Jiadi Xu, Kenichi L. Ishikawa, Hide Takagi, Minoru Nohara, Naoyuki Katayama, Hiroshi Sawa, Masami Fujisawa, Teruto Kanai, Jiro Itatani, Takashi Mizokawa, Shik Shin, and Kozo Okazaki

Phys. Rev. B **103**, L121105 — Published 10 March 2021

DOI: [10.1103/PhysRevB.103.L121105](https://doi.org/10.1103/PhysRevB.103.L121105)

Detecting electron-phonon couplings during photo-induced phase transition

Takeshi Suzuki^{1,*}, Yasushi Shinohara^{2,3}, Yangfan Lu⁴, Mari Watanabe¹, Jiadi Xu¹, Kenichi L. Ishikawa^{2,3,5}, Hide Takagi^{4,6}, Minoru Nohara⁷, Naoyuki Katayama⁸, Hiroshi Sawa⁸, Masami Fujisawa¹, Teruto Kanai¹, Jiro Itatani¹, Takashi Mizokawa⁹, Shik Shin^{1,10,11,*}, and Kozo Okazaki^{1,10,*}

¹*Institute for Solid State Physics, The University of Tokyo, Kashiwa, Chiba 277-8581, Japan*

²*Photon Science Center, Graduate School of Engineering, The University of Tokyo, 7-3-1 Hongo, Bunkyo-ku, Tokyo 113-8656, Japan*

³*Department of Nuclear Engineering and Management, Graduate School of Engineering, The University of Tokyo, 7-3-1, Hongo, Bunkyo-ku, Tokyo 113-8656, Japan*

⁴*Department of Physics, University of Tokyo, Hongo, Tokyo, 113-0033, Japan*

⁵*Research Institute for Photon Science and Laser Technology, The University of Tokyo, 7-3-1 Hongo, Bunkyo-ku, Tokyo 113-0033, Japan*

⁶*Max Planck Institute for Solid State Research, Heisenbergstrasse 1, 70569 Stuttgart, Germany*

⁷*Research Institute for Interdisciplinary Science, Okayama University, Okayama, 700-8530, Japan*

⁸*Department of Applied Physics, Nagoya University, Nagoya 464-8603, Japan*

⁹*School of Advanced Science and Engineering, Waseda University, Shinjuku, Tokyo 169-8555, Japan*

¹⁰*AIST-UTokyo Advanced Operando-Measurement Technology Open*

Innovation Laboratory (OPERAND-OIL), Kashiwa, Chiba 277-8581, Japan

¹¹*Office of University Professor, The University of Tokyo, Kashiwa, Chiba 277-8581, Japan*

(Dated: February 5, 2021)

Photo-induced phase transitions have been intensively studied owing to the ability to control a material of interest in the ultrafast manner, which can induce exotic phases unable to be attained at equilibrium. However, the key mechanisms are still under debate, and it has currently been a central issue how the couplings between the electron, lattice, and spin degrees of freedom are evolving during photo-induced phase transitions. Here, we use a recently developed analysis method, which we call frequency-domain angle-resolved photoemission spectroscopy (FDARPES), and reveal mode- and band-selective electron-phonon couplings during the photo-induced insulator-to-metal transition for Ta₂NiSe₅. We find that the lattice modulation corresponding to the 2 THz phonon mode, where Ta lattice is sheared along the a-axis, is the most relevant for the photo-induced semimetallic state. Furthermore, we find that the semimetallic and semiconducting bands coexist in the transient state, and demonstrate that FDARPES spectra can detect the phonon-specific couplings to the two coexistent band structures during the photo-induced phase transition selectively by resolving them in the frequency domain.

Strongly-correlated electron systems display very rich phases owing to intertwined couplings between multiple degrees of freedom including the charge, orbital, spin, and lattice [1]. Moreover, external fields, such as electronic and magnetic fields or physical pressure, can induce phase transitions in these systems by breaking their subtle balances between multiple competing phases [2, 3]. In this respect, photo-excitation is a very promising way to control the physical properties because it can instantaneously change physical properties of a targeting material in various manners by exploiting many degrees of freedom such as polarization or wavelength [4]. For studying photo-excited nonequilibrium states, time- and angle-resolved photoemission spectroscopy (TARPES) has a strong advantage because it can track nonequilibrium electronic band structures after photoexcitations [5–8].

For photo-induced phase transitions, although many strongly-correlated electron systems have been intensively studied [9–13], the precise mechanisms are still under debate [14–16]. Recently, we revealed the photo-induced insulator-to-metal transitions (IMTs) in

Ta₂NiSe₅ [17], where we also showed strong evidence in dynamical behaviors as an excitonic insulator. Moreover, other interesting photo-excited phenomena in Ta₂NiSe₅ have been reported previously, which include photo-induced enhancement of the excitonic insulator [18, 19] or emergence of collective modes [20, 21]. In most reports, the key roles for such phenomena are played by significant electron-phonon couplings.

Recently, a new analysis method of mapping the Fourier component of TARPES in energy and momentum axis was reported to reveal electron-phonon couplings in *Td*-WTe₂ [22]. By this method they successfully extracted the mode-specific phonon coupling to the electronic band structure, and revealed the new aspects for the Weyl physics. Later, this method was theoretically investigated to microscopically show how the intensity and phase of a spectrum is related to the electron-phonon coupling matrix elements [23].

In this Letter, we report that this fairly new analysis method, which we call frequency-domain angle-resolved photoemission spectroscopy (FDARPES), can

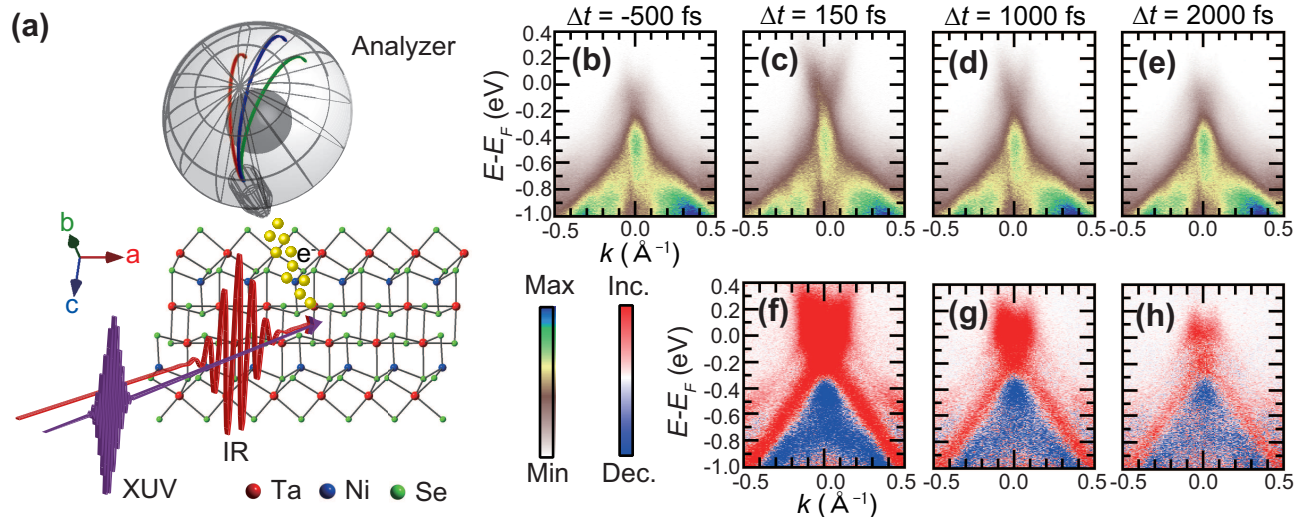


FIG. 1. (a) Schematic illustration of time- and angle-resolved photoemission spectroscopy (TARPES), as applied to Ta₂NiSe₅. The pump pulse is infrared light whereas the probe pulse is extreme ultraviolet light produced by high-harmonic generation. Photoelectrons are detected by a hemisphere analyzer. (b)-(e) TARPES spectra of Ta₂NiSe₅. The delay time between the pump and probe is indicated in each panel. (f)-(h) Difference images of TARPES. Red and blue points represent increasing and decreasing photoemission intensity, respectively.

be used to measure mode- and band-selective electron-phonon couplings during the photo-induced insulator-to-metal phase transition in Ta₂NiSe₅. We observe that the lattice modulation corresponding to the phonon mode, where Ta lattice is sheared along the a-axis, is the most relevant for the photo-induced semimetallic state. By using FDARPES method, we also find that the semimetallic and semiconducting bands coexist during the photo-induced phase transition. Furthermore, FADRPES spectra can detect the phonon-specific couplings to the semimetallic and semiconducting bands selectively during the photo-induced phase transition by distinguishing them in the frequency domain.

TARPES, as illustrated in Fig. 1(a), allows us to directly observe the temporal evolution of the electronic band structure. We used an extremely stable commercial Ti:sapphire regenerative amplifier system (Spectra-Physics, Solstice Ace) with a center wavelength of 800 nm, a repetition rate of 10 kHz, and pulse width of ~ 35 fs for the pump pulse. Second harmonic pulses generated in a 0.2-mm-thick crystal of β -BaB₂O₄ were focused into a static gas cell filled with Ar to generate higher harmonics. By using a set of SiC/Mg multilayer mirrors, we selected the seventh harmonic of the second harmonic ($h\nu = 21.7$ eV) for the probe pulse. The temporal resolution was determined to be ~ 70 fs from the TARPES intensity far above the Fermi level, which corresponded to the cross correlation between the pump and probe pulses. The hemispherical electron analyzer (Omicron-Scientia R4000) is used to detect photoelectrons. The overall energy resolution is set to be 250 meV. All the measurements in this work were performed at the tem-

perature of 100 K.

The sample is a high-quality single crystals of Ta₂Ni(Se_{0.97}S_{0.03})₅ grown by chemical vapour transport method using I₂ as transport agent, as was reported in the refs [24, 25]. Whereas a relatively large cleaved surface is necessary for TARPES measurements compared with static ARPES, because Ta₂NiSe₅ has a one-dimensional crystal structure, a large cleaved surface of the pristine Ta₂NiSe₅ that was sufficient for TARPES measurements was difficult to obtain. However, sufficiently-large cleaved surface of 3 % S-substituted Ta₂NiSe₅ could be obtained. This is why we used 3 % S-substituted Ta₂NiSe₅ rather than pristine Ta₂NiSe₅ in this study. Clean surfaces were obtained by cleaving in situ.

Figures 1(b)-1(e) show the TARPES snapshots of Ta₂NiSe₅ at various delays shown as a function of momentum and energy. The pump fluence is set to be 2.27 mJ/cm². The delay between the pump and probe (Δt) is indicated in each panel. To enhance the temporal variations, the difference images between the before and after photoexcitation are shown in Figs. 1(f)-1(h), where red and blue represent an increase and decrease in photoemission intensity, respectively. After strong photoexcitation, new semimetallic electron- and hole-dispersions appear, as has previously been reported [17]. This is the direct signature of photo-induced IMT. To highlight the change of the electronic band structure, we show the peak positions of the TARPES spectra before and after photoexcitation in Figs. 2(a) and 2(b), which are averaged at $\Delta t = [-800, -200]$ fs and $[300, 1900]$ fs, respectively. One can notice that the hole band is shifted upward and crosses

the Fermi level, E_F , while the electron band appears and crosses E_F at the same Fermi wavevector, k_F , as the hole band. Sizable spectral weights above E_F in Figs. 1(b) and 2(a) seem to be due to the relatively worse energy resolution compared to the static ARPES measurement. We also check there is negligible thermal effect before the arrival of pump by comparing the photoemission spectrum at the negative delay with that without pump as shown in Fig. S1.

To more specifically reveal the photo-induced profile in Ta_2NiSe_5 , we investigated the TARPES images in terms of electron-phonon couplings. Figure 2(c) shows the time-dependent intensities for representative regions in the energy and momentum space indicated as I-IV in Figs. 2(a) and 2(b). As a background, carrier dynamics

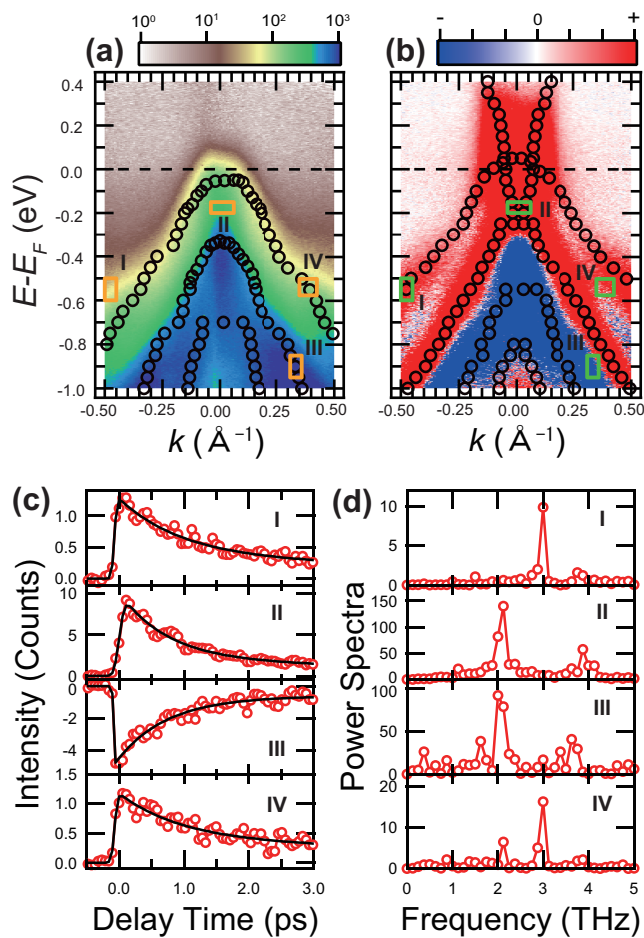


FIG. 2. TARPES spectra (a) before and (b) after pump excitation. The peak positions in the TARPES spectra are indicated as circles. (c) Time-dependent TARPES intensities at different energy and momentum regions. I-IV corresponds to the regions indicated in (a) and (b). Data are shown as red circles whereas the fitting results by double-exponential decay functions convoluted with a Gaussian function are shown as black solid lines. (d) Intensities of Fourier transforms of the oscillation components in (c) I-(c) IV obtained by subtracting the fitting curve from the data.

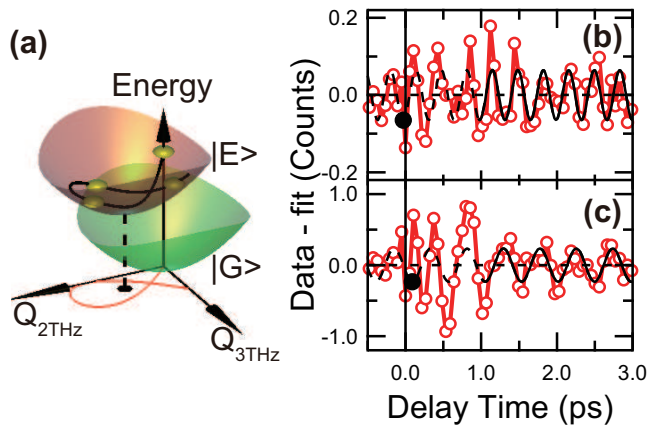


FIG. 3. (a) Schematic illustration of the free energy curves for the ground and photo-excited states as a function of lattice coordinates corresponding to the directions of the 2-THz and 3-THz phonon modes. (b), (c) Oscillation components for I and II corresponding to the data subtracted by the fits. The fitting curve using a single cosine function are shown as dotted and solid black curves. We use data for the fits shown by solid black curves.

corresponding to overall rise-and-decay or decay-and-rise behaviors were observed. Additionally, oscillatory behaviors were clearly seen superimposed onto background carrier dynamics, which indicated strong electron-phonon couplings as a result of excitations of coherent phonons. To extract the oscillatory components, we first fit the carrier dynamics to a double-exponential function convoluted with a Gaussian function, shown as the black-solid lines in Fig. 2(c), and then subtracted the fitting curves from the data. Fourier transformations were performed for the subtracted data and the intensities for each frequency component are shown in Fig. 2(d). One can clearly see that distinctively different frequency-dependent peak structures appeared depending on the regions in the energy and momentum space denoted as I-IV in Figs. 2(a) and 2(b).

Considering that the frequencies for the peak positions observed in this work matched the A_g phonon modes reported in previous work [26, 27] and that we dominantly excited the electron system under our experimental condition, the observed coherent phonons were likely to arise from displacive excitation of coherent phonons (DECPs) [28]. According to the DECP theory, photoexcitation suddenly changes the minimum energy position in the lattice coordinates of the potential energy surface (PES), and lattice coordinates oscillate around the new energy minimum position with its own frequency determined by the curvature of the PES. Figure 3(a) schematically shows this situation. The PESs for the ground and excited states are denoted as $|G\rangle$ and $|E\rangle$, respectively, and $Q_{2\text{THz}}$ and $Q_{3\text{THz}}$ are the lattice coordinates corresponding to the 2-THz and 3-THz phonon modes. It should be noted that the minimum energy positions of

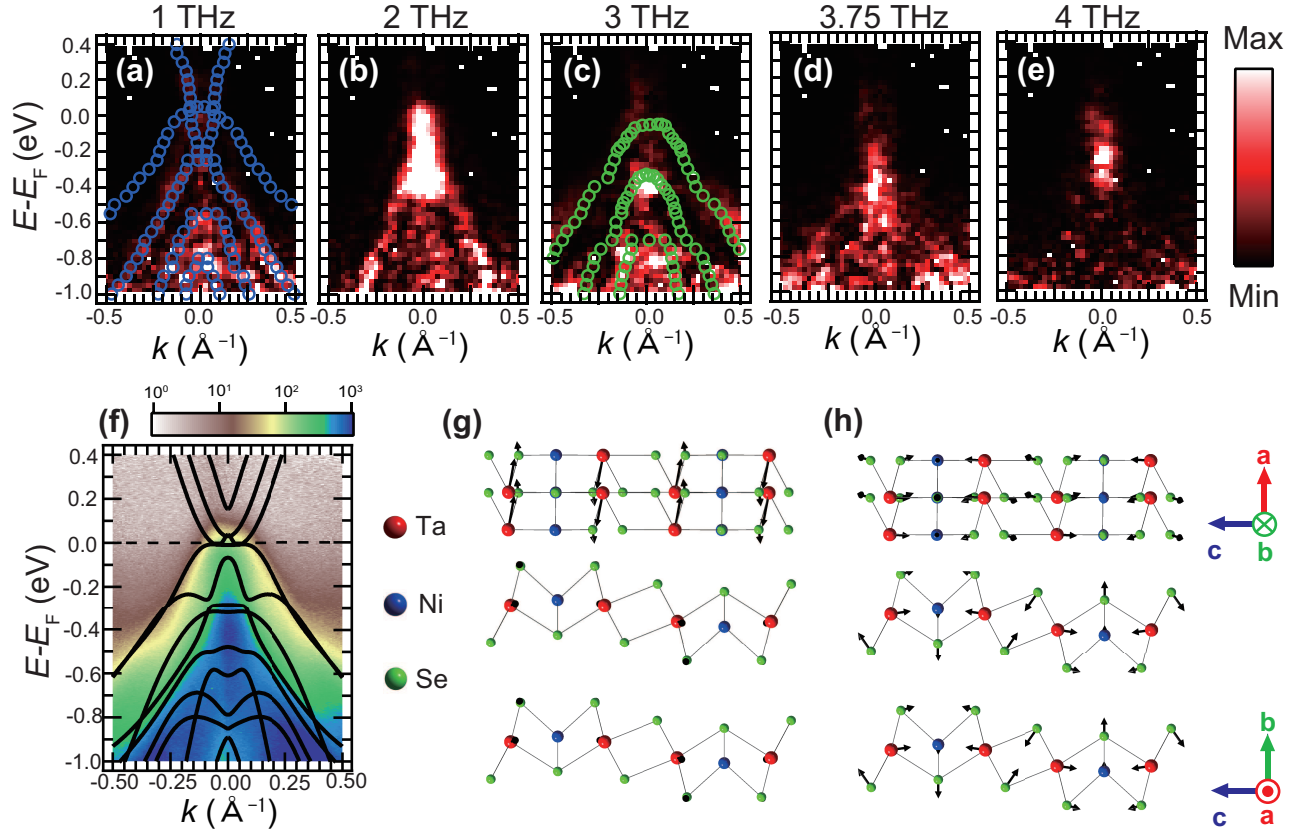


FIG. 4. (a)-(e) Frequency-domain angle-resolved photoemission spectroscopy (FDARPES) spectra shown as frequency-dependent intensities of the oscillation components as a function of energy and momentum. The peak positions in the TARPEs spectra after and before photoexcitation are plotted as blue and green circles in Fig. 4(a) and Fig. 4(c), respectively. (f) Calculated band structure of Ta_2NiSe_5 based on the density-functional theory with GGA functional superimposed onto the photoemission spectrum before pump excitation. (g), (h) Calculated phonon modes corresponding to (b) and (c), respectively.

the PESs for the ground and excited states are different, *i.e.* the minimum energy position for the excited state have finite values of $Q_{2\text{THz}}$ and $Q_{3\text{THz}}$ shown as the black dot on the $(Q_{2\text{THz}}, Q_{3\text{THz}})$ plane while that for the ground state corresponds to the origin ($Q_{2\text{THz}} = Q_{3\text{THz}} = 0$). It should also be mentioned that while the actual PES is expressed in multi lattice coordinates corresponding to each phonon mode, here we only include 2 modes to provide the visual image. The dynamics of the lattice coordinates is expressed by motion of the yellow ball and its trajectory is shown as the black solid curve (the red solid curve) on the PES of the excited state (for the projection onto the $(Q_{2\text{THz}}, Q_{3\text{THz}})$ plane).

To investigate the phases of coherent phonons, we further fitted the oscillatory components by single-cosine function. Figures 3(b) and 3(c) shows the results for regions I and II, in which the 3- and 2-THz components exhibited the strongest peaks, respectively. Phases and frequencies were obtained as $0.19 \pm 0.11 \pi$ and 2.97 ± 0.02 THz for region I, and $0.37 \pm 0.12 \pi$ and 2.07 ± 0.02 THz for region II, respectively. If the change of PES accompanies no delay from the laser excitation, DECP has a

cosine-like behavior, that is, the expected phase is 0π . Thus, the modulation of photoemission intensity in region I along the 3-THz phonon mode was triggered immediately after photoexcitation. On the other hand, the relatively positive phase shift in region II compared with region I indicated the modulation of the photoemission intensity along the 2-THz phonon mode occurred with a delay of 120 fs.

We will now discuss the electron-phonon couplings in more detail. Since we observed that the amplitude of each oscillation significantly changed depending on the regions in the energy and momentum space, we further mapped out the frequency-dependent intensity of the Fourier component in the energy and momentum space, which we call FDARPES. Figures 4(a)-4(e) show the FDARPES spectra corresponding to the frequencies of 1, 2, 3, 3.75, and 4 THz, respectively. In order to see each phonon mode associated with the FDARPES spectra, we perform ab initio calculations. First, we calculate the band structure for Ta_2NiSe_5 by using density-functional theory with GGA functional and confirm that the results can overall reproduce the photoemission spec-

trum shown in Fig. 4(f). Then, we employ the density-functional perturbation theory to obtain phonon modes. The phonon modes corresponding to 2 and 3 THz are shown in Figs. 4(g) and 4(h). The full results of phonon modes and details of calculations are found in Supplemental Material [29]. We assigned all the phonon modes as A_g modes in the monoclinic phase. In the previous results of Raman measurements at different polarization settings [21], eleven Raman-active phonon modes are observed in the Y(ZZ)Y setting while the three of them show stronger peak intensities in the Y(ZX)Y than in the Y(ZZ)Y. This is considered to be due to the fact that all of the observed modes have A_g character in the monoclinic phase and three of them turn to be B_{2g} character in the orthorhombic phase. Precise procedures of phonon assignments are found in Supplemental Material [29].

Noticeably, the FDARPES spectra exhibit distinctively different behaviors depending on the frequency, which demonstrates that each phonon mode is selectively coupled to the specific electronic bands. Particularly, the 2-THz phonon mode has the strongest signal around E_F , where it consists of a mixture of Ta $5d$ and Se $3p$ orbitals [45], and this signature is responsible for the collapse of the excitonic insulator. **Because recent theoretical investigation reported that the intensity of FDARPES spectra is expressed as the sum of two terms proportional to diagonal and off-diagonal electron-phonon coupling matrix elements under the condition of large pulse dependent spectral linewidth [23], this strongest signal suggests that the 2 THz-phonon mode is most strongly coupled to the emergent photo-induced electronic bands crossing E_F .**

In order to see spectral features of FDARPES in more detail, we compare the FDARPES spectra with the band dispersions before and after photoexcitation. Full results are found in Fig. S4 [29]. We find that FDARPES spectrum at 1 THz matches the band dispersions after photoexcitation better than that before photoexcitation shown in Fig. 4(a) while the FDARPE spectrum at 3 THz is closer to the band dispersions before photoexcitation shown in Fig. 4(c). This means that both semimetallic and semiconducting bands are coexistent in the transient state, and suggests the strong electron-phonon couplings for 1- and 3-THz phonon modes are associated with semimetallic and semiconducting bands, respectively. Moreover, this finding demonstrates that whereas semimetallic and semiconducting states coexist after photo-excitation, the FDARPES method can selectively reveal the coupling of each phonon mode to semimetallic and semiconducting states owing to the frequency-resolved manner. **Regarding the lifetime of coherent phonons, we focus on the linewidths of power spectra lying at the semiconducting and semimetallic bands, which correspond to the region II and IV in Fig. 2, respectively. It is noticed that the linewidth at 3 THz shown in Fig. 2(d)-IV is smaller than that at 2 THz**

shown in Fig. 2(d)-II, which suggests that the coherent phonons coupled to the semiconducting states are more stabilized.

As clearly seen in this work, our employed analysis method, FDARPES, can detect the mode- and band-selective electron-phonon couplings during the photo-induced phase transition. Our work using this method provides direct evidence for the DECP mechanisms responsible for the photo-induced IMTs in Ta_2NiSe_5 . Thus, FDARPES can be used to study many other photo-induced phase transitions by observing how the electron band structure is influenced by the specific phonon-mode. We also emphasize the versatility of FDARPES. By using the multiple degrees of freedom in the excitation pulses, we can drive different quasiparticles; for example, circularly-polarized pulses can promote a specific spin population or appropriate mid- and far-infrared wavelength can resonantly excite IR-active phonons. Furthermore, FDARPES can detect couplings of electrons to any quasiparticles or collective modes as long as their couplings manifest as oscillations of intensities in the TARPES spectra.

We would like to acknowledge Y. Ohta, for valuable discussions and comments. This work was supported by Grants-in-Aid for Scientific Research (KAKENHI) (Grant No. JP18K13498, JP19H00659, JP19H01818, JP19H00651 JP18K14145, and JP19H02623) from the Japan Society for the Promotion of Science (JSPS), by JSPS KAKENHI on Innovative Areas Quantum Liquid Crystals (Grant No. JP19H05826), by the Center of Innovation Program from the Japan Science and Technology Agency, JST, the Research and Education Consortium for Innovation of Advanced Integrated Science by JST, and by MEXT Quantum Leap Flagship Program (MEXT Q-LEAP) (Grant No. JPMXS0118067246, JPMXS0118068681), Japan. The computation in this work has been done using the facilities of the Supercomputer Center, The Institute for Solid State Physics, The University of Tokyo.

-
- [1] Y. Tokura, M. Kawasaki, and N. Nagaosa, *Nat. Phys.* **13**, 1056 (2017).
 - [2] B. Wu, A. Zimmers, H. Aubin, R. Ghosh, Y. Liu, and R. Lopez, *Phys. Rev. B* **84**, 241410(R) (2011).
 - [3] K. Matsuura, Y. Mizukami, Y. Arai, Y. Sugimura, N. Maejima, A. Machida, T. Watanuki, T. Fukuda, T. Yajima, Z. Hiroi, *et al.*, *Nat. Commun.* **8**, 1143 (2017).
 - [4] D. N. Basov, R. D. Averitt, and D. Hsieh, *Nat. Mat.* **16**, 1017 (2017).
 - [5] T. Rohwer, S. Hellmann, M. Wiesenmayer, C. Sohrt, A. Stange, B. Slomski, A. Carr, Y. Liu, L. M. Avila, M. Kallane, *et al.*, *Nature* **471**, 490 (2011).
 - [6] S. Hellmann, T. Rohwer, M. Kalläne, K. Hanff, C. Sohrt, A. Stange, A. Carr, M. M. Murnane, H. C. Kapteyn, L. Kipp, *et al.*, *Nat. Commun.* **3**, 1069 (2012).

- [7] F. Schmitt, P. S. Kirchmann, U. Bovensiepen, R. G. Moore, L. Rettig, M. Krenz, J.-H. Chu, N. Ru, L. Perfetti, L. D. H. Lu, *et al.*, *Science* **321**, 1649 (2008).
- [8] T. Suzuki, T. Iimori, S. J. Ahn, Y. Zhao, M. Watanabe, J. Xu, M. Fujisawa, T. Kanai, N. Ishii, J. Itatani, *et al.*, *ACS Nano* **13**, 11981 (2019).
- [9] K. Miyano, T. Tanaka, Y. Tomioka, and Y. Tokura, *Phys. Rev. Lett.* **78**, 4257 (1997).
- [10] E. Collet, M.-H. Lemée-Cailleau, M. B.-L. Cointe, H. Cailleau, M. Wulff, T. Luty, S.-Y. Koshihara, M. Meyer, L. Toupet, P. Rabiller, *et al.*, *Science* **300**, 612 (2003).
- [11] D. Fausti, R. I. Tobey, N. Dean, S. Kaiser, A. Dienst, M. C. Hoffmann, S. Pyon, T. Takayama, H. Takagi, and A. Cavalleri, *Science* **331**, 189 (2011).
- [12] T. Frigge, B. Hafke, T. Witte, B. Krenzer, C. Streubühr, S. A. Samad, T. V. Mikšić, I. Avigo, P. Zhou, M. Ligges, *et al.*, *Nature* **544**, 207 (2017).
- [13] A. Zong, A. Kogar, Y.-Q. Bie, T. Rohwer, C. Lee, E. Baldini, E. Ergeen, M. B. Yilmaz, B. Freelon, E. J. Sie, *et al.*, *Nat. Phys.*, **15**, 27 (2019).
- [14] N. Gedik, D.-S. Yang, G. Logvenov, I. Bozovic, A. H. Zewail, *Science* **316**, 425 (2007).
- [15] V. R. Morrison, R. P. Chatelain, K. L. Tiwari, A. Hendaoui, A. Bruhcs, M. Chaker, and B. J. Siwick, *Science* **346**, 445 (2014).
- [16] H. Ichikawa, S. Nozawa, T. Sato, A. Tomita, K. Ichiyanaqi, M. Chollet, L. Guerin, N. Dean, A. Cavalleri, S. Adachi, *et al.*, *Nat. Mater.* **10**, 101 (2011).
- [17] K. Okazaki, Y. Ogawa, T. Suzuki, T. Yamamoto, T. Someya, S. Michimae, M. Watanabe, Y. Lu, M. Nohara, H. Takagi, *et al.*, *Nat. Commun.* **9**, 4322 (2018).
- [18] S. Mor, M. Herzog, D. Golež, P. Werner, M. Eckstein, N. Katayama, M. Nohara, H. Takagi, T. Mizokawa, C. Monney, *et al.*, *Phys. Rev. Lett.* **119**, 086401 (2017).
- [19] T. Tanabe, K. Sugimoto, and Y. Ohta, *Phys. Rev. B* **98**, 235127 (2018).
- [20] Y. Murakami, D. Golež, M. Eckstein, and P. Werner, *Phys. Rev. Lett.* **119**, 247601 (2017).
- [21] D. Werdehausen, T. Takayama, M. Höppner, G. Albrecht, A. W. Rost, Y. F. Lu, D. Manske, H. Takagi, and S. Kaiser, *Sci. Adv.* **4**, eaap8652 (2018).
- [22] P. Hein, S. Jauernik, H. Erk, L. Yang, Y. Qi, Y. Sun, C. Felser, M. Bauer, *Nat. Commun.* **11**, 2613 (2020).
- [23] **U. De Giovannini, H. Hübener, S. A. Sato, and A. Rubio, *Phys. Rev. Lett.* **125**, 136401 (2020).**
- [24] Y. F. Lu, H. Kono, T. I. Larkin, A. W. Rost, T. Takayama, A. V. Boris, B. Keimer, and H. Takagi, *Nat. Commun.* **8**, 14408 (2017).
- [25] A. Nakano, K. Sugawara, S. Tamura, N. Katayama, K. Matsubayashi, T. Okada, Y. Uwatoko, K. Munakata, A. Nakao, H. Sagayama, *et al.*, *IUCrJ* **5**, 158 (2018).
- [26] S. Y. Kim, Y. Kim, C.-J. Kang, E.-S. An, H. K. Kim, M. J. Eom, M. Lee, C. Park, T.-H. Kim, H. C. Choi, *et al.*, *ACS Nano* **10**, 8888 (2016).
- [27] S. Mor, M. Herzog, J. Noack, N. Katayama, M. Nohara, H. Takagi, A. Trunschke, T. Mizokawa, C. Monney, and J. Stähler, *Phys. Rev. B* **97**, 115154 (2018).
- [28] H. J. Zeiger, J. Vidal, T. K. Cheng, E. P. Ippen, G. Dresselhaus, and M. S. Dresselhaus, *Phys. Rev. B* **45**, 768 (1992).
- [29] See Supplemental Material at <http://link.aps.org/supplemental/> for details of the theoretical method and the comparison of band dispersions and FDARPES spectra, which includes additional Refs. [30] [44].
- [30] O. V. Misochko and M. V. Lebedev *J. Exp. Theor. Phys.* **126**, 64 (2018).
- [31] G. A. Garrett, T. F. Albrecht, J. F. Whitaker, and R. Merlin, *Phys. Rev. Lett.* **77**, 3661 (1996).
- [32] K. Ishioka, M. Kitajima, and O. V. Misochko, *J. of Appl. Phys.* **103**, 123505 (2008).
- [33] P. Hohenberg and W. Kohn, *Phys. Rev.* **136**, B864 (1964).
- [34] W. Kohn and L. J. Sham, *Phys. Rev.* **140**, A1133 (1965).
- [35] J. P. Perdew, K. Burke, and M. Ernzerhof, *Phys. Rev. Lett.* **77**, 3865 (1996).
- [36] X. Gonze, F. Jollet, A. F. Abreu, D. Adams, B. Amadon, T. Applencourt, C. Audouze, J.-M. Beuken, J. Bieder, A. Bokhanchuk, *et al.*, *Comput. Phys. Commun.* **205**, 106 (2016).
- [37] M. Fuchs and M. Scheffler, *Comput. Phys. Commun.* **119**, 67 (1999).
- [38] https://www.abinit.org/sites/default/files/PrevAtomicData/psp-links/gga_fhi.html
- [39] S. A. Sunshine and J. A. Ibers, *Inorg. Chem.* **24**, 3611 (1985).
- [40] B. S. de Gironcoli, A. Dal Corso, and P. Giannozzi, *Rev. Mod. Phys.* **73**, 515 (2001).
- [41] J. P. Perdew and Y. Wang, *Phys. Rev. B* **45**, 13244 (1992).
- [42] https://www.abinit.org/sites/default/files/PrevAtomicData/psp-links/lda_fhi.html
- [43] K. Seki, Y. Wakisaka, T. Kaneko, T. Toriyama, T. Konishi, T. Sudayama, N. L. Saini, M. Arita, H. Namatame, M. Taniguchi, N. Katayama, M. Nohara, H. Takagi, T. Mizokawa, and Y. Ohta, *Phys. Rev. B* **90**, 155116 (2014).
- [44] T. Kaneko, T. Toriyama, T. Konishi, and Y. Ohta, *Phys. Rev. B* **87**, 035121 (2013).
- [45] J. Lee, C. -J. Kang, M. J. Eom, J. S. Kim, B. I. Min, and H. W. Yeom, *Phys. Rev. B* **99**, 075408 (2019).